

Rib cortical bone thickness variation in adults by age and sex

Sven A. Holcombe  | Brian A. Derstine 

Morphomics Analysis Group, University of Michigan, Ann Arbor, Michigan, USA

Correspondence

Sven A. Holcombe, Morphomics Analysis Group, University of Michigan, Ann Arbor, MI, USA.

Email: svenho@umich.edu**Abstract**

Rib fractures are a common and serious outcome of blunt thoracic trauma and their likelihood is greater in older individuals. Osteoporotic bone loss is a well-documented aging phenomenon with sex-specific characteristics, but within rib bones, neither baseline maps of regional thickness nor the rates of bone thinning with age have been quantified across whole ribs. This study presents such data from 4014 ribs of 240 adult subjects aged 20–90. A validated cortical bone mapping technique was applied to clinical computed tomography scans to obtain local rib cortical bone thickness measurements over the surfaces of ribs 2 through 11. Regression models to age and sex gave rates of cortex thinning in local zones and aggregated across whole ribs. The statistical parametric mapping provided these relationships regionally as a function of rib surface location. All models showed significant reductions in bone thickness with age ($p < 0.01$). Average whole-rib thinning occurred at between 0.011 to 0.032 mm/decade (males) and 0.035 to 0.043 mm/decade (females), with sex and age accounting for up to 37% of population variability (R^2). Rates of thinning differed regionally and by rib, with the highest bone loss of up to 0.074 mm/decade occurring in mid-rib cutaneous and superior regions of ribs 2–6. Rates were consistently higher in females than males (significantly so across whole ribs but not all local regions) and were more pronounced in cutaneous, superior, and inferior rib aspects (average 0.025 mm/decade difference in ribs 4–8) compared to pleural aspects which had the thickest cortices but saw only minor differences in thinning rates by sex (0.045 mm/decade for females and 0.040 mm/decade for males). Regional analysis showed male and female bone thickness differences that were not statistically significant at 20 years of age ($p > 0.05$ across practically all regions) but subsequent cortex thinning meant that substantial pleural and cutaneous regions were thinner ($p < 0.05$) in females than males by 55 years of age. The techniques and results from this study can be applied to assess rib bone content loss in clinical settings across wide populations. Additionally, average cortex thickness results can be mapped directly to finite element models of the thorax, and regression results are used to modify such models to represent the ribs of men and women across their full adult lifespan.

KEYWORDS

computational models, computed tomography, cortical bone, cortical thickness, rib

1 | INTRODUCTION

Thoracic injuries are a major concern in trauma and the ribs play a key protective and structural role. Rib fractures are the most commonly occurring thoracic injury, and their presence acts as a sentinel for further injury to critical organs in the chest and abdomen (Dogrul et al., 2020; Talbot et al., 2017; Witt & Bulger, 2017). Occupant protection in motor vehicle crashes has improved considerably over previous eras, but rib fracture rates have seen only marginal reductions during this time and remain as the most common serious injury in multiple crash scenarios (Forman et al., 2019; Pipkorn et al., 2020). With changing population demographics, there is further concern not just with increased rib fracture frequency with age, but also with higher resulting mortality and morbidity in the elderly and other vulnerable populations (Sirmali et al., 2003; Stawicki et al., 2004). Osteoporosis is a skeletal disorder seen in all populations but with the highest incidences among older people, Caucasians, and women (Alswat, 2017; Sozen et al., 2017). It is characterized by decreased bone mass and a deteriorated bone microstructure that results in reduced bone strength, elevated bone fragility, and increased fracture risk (Chen, 2014). Bone loss mechanisms and rates with aging are well documented in multiple body regions including the pelvis, femoral heads, vertebrae, and wrists, and similar trends are expected to be found in the ribs (Eftekhar-Sadat et al., 2016; Pignolo et al., 2021; Poole et al., 2012; Telfer et al., 2021).

Computational human body models (HBMs) are a tool for simulating and predicting injury under a wide range of loading conditions. They are generally built to target one specific demographic (e.g., 50th percentile male), and most efforts to broaden their applicability to better represent subjects of varying sex and age involve post-hoc morphing of their geometry based on reference literature (Chen et al., 2018; Holcombe et al., 2017; Hwang et al., 2020; Schoell et al., 2015; Shi et al., 2014; Vavalle et al., 2014). Predicting rib fracture events with HBMs is a particularly difficult task, and rib-only models that introduce detailed rib-specific geometry and bone thickness have found improved accuracy in such predictions (Iraeus et al., 2019; Li et al., 2010). Most full-body HBMs, however, have simplified rib geometry that deviates substantially from typical anatomy of their target demographic (Holcombe et al., 2020), stemming in part from insufficiently detailed anatomical reference data at the time of construction.

Rib bone properties including cortex thickness play a key role in fracture events and show large inter-subject variation as well as regional variation across the rib cage (Agnew et al., 2018; Kemper et al., 2005, 2007; Murach et al., 2017). Rib cortical thickness has been measured to span approximately 0.1–2.6 mm (Agnew et al., 2018; Choi & Kwak, 2011; Holcombe, Kang, Derstine, et al., 2019; Mohr et al., 2007), but these data are limited to individual rib levels or sites, or have been aggregated across broad regions containing wide ranges of variation. To date, thickness measurements across multiple levels and in sufficient detail for direct application to HBMs has not yet been expounded in the literature. This study aims firstly to address this knowledge gap, and secondly to investigate regional relationships between cortex thickness and subject age and sex.

2 | MATERIALS AND METHODS

Chest computed tomography (CT) scans of 240 females and males between 20 and 90 years of age (15 or more subjects per sex per decade) were obtained from within the University of Michigan morphomics database under IRB HUM00041441. Subject demographic distributions in age (avg \pm SD of 55 ± 19 years), height, weight, and body mass index are shown in Figure 1. Self-reported subject race or ethnicity was Caucasian (80%), African American (10%), Asian (2%), Hispanic or Latino (2%), or unreported (6%). All scans were acquired as part of standard trauma diagnosis and care at 0.625 mm slice spacing using a standard reconstruction kernel optimized for visualizing soft tissue. Axial resolution within each scan ranged between 0.50 mm/px and 0.97 mm/px. Subjects had normal thoracic skeletal anatomy and fractured ribs were excluded from the study.

2.1 | Image processing

Three-dimensional (3D) centerline curves were placed along all ribs within each scan and a series of planar rectangular patch areas (10 mm by 20 mm) were defined perpendicular to each rib at 2.5% intervals along its central curve (Figure 2). The local X-axis of each patch was oriented to best align to the local pleural-to-cutaneous direction (i.e., perpendicular to the chest wall), defined by the normal direction of a 3D spline surface fitted to the collection of all rib curves in each scan.

The sequence of steps illustrated in Figure 3 was applied to each individual patch as described below. Firstly, thresholding and morphological operations produced an initial binary segmentation, and a periodic spline was fitted to its outer perimeter (Figure 3b). To counter known over-segmentation issues arising from thresholding (Holcombe, Kang, Derstine, et al., 2019; Holcombe, Kang, Wang, & Agnew, 2019), an initial pass of the cortical bone mapping algorithm (CBM, see Holcombe et al., 2018; Treece & Gee, 2015; for details) was applied perpendicular to points along this spline to shift it along its normal direction to better align with the true cortex border (Figure 3c). A second CBM pass was then performed on cross-cortex samples (Figure 3d) at 40 equally spaced points around the rib to provide initial estimates of periosteal and endosteal borders (Figure 3e). This output was filtered to avoid dual-cortex issues prevalent near the costal groove (Holcombe, Kang, Derstine, et al., 2019), and a smoothing spline was fitted to provide final periosteal and endosteal borders (Figure 3f). The shortest distance between these borders gave the local cortical bone thickness (Ct.Th) as a continuous function around the rib. Ct.Th measures were retained only when the vector from the periosteal border to its nearest location on the endosteal border matched the normal direction of the periosteal border to within 20°.

Four landmarks were identified on each patch to provide inter-subject registration in the around-rib direction. These started with an inferior landmark at the inferior-most point of the periosteal border

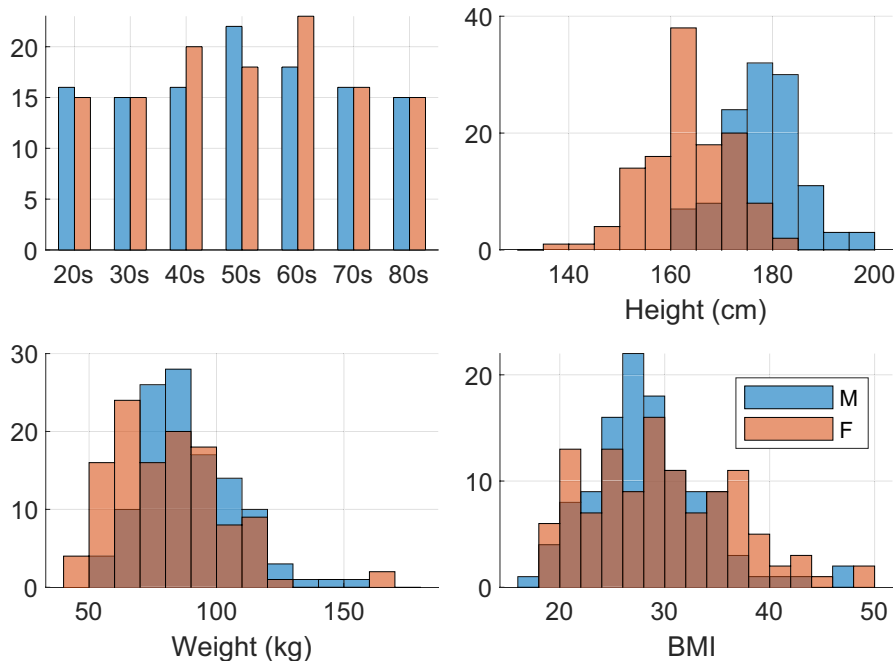


FIGURE 1 Histogram distributions of subject demographics.

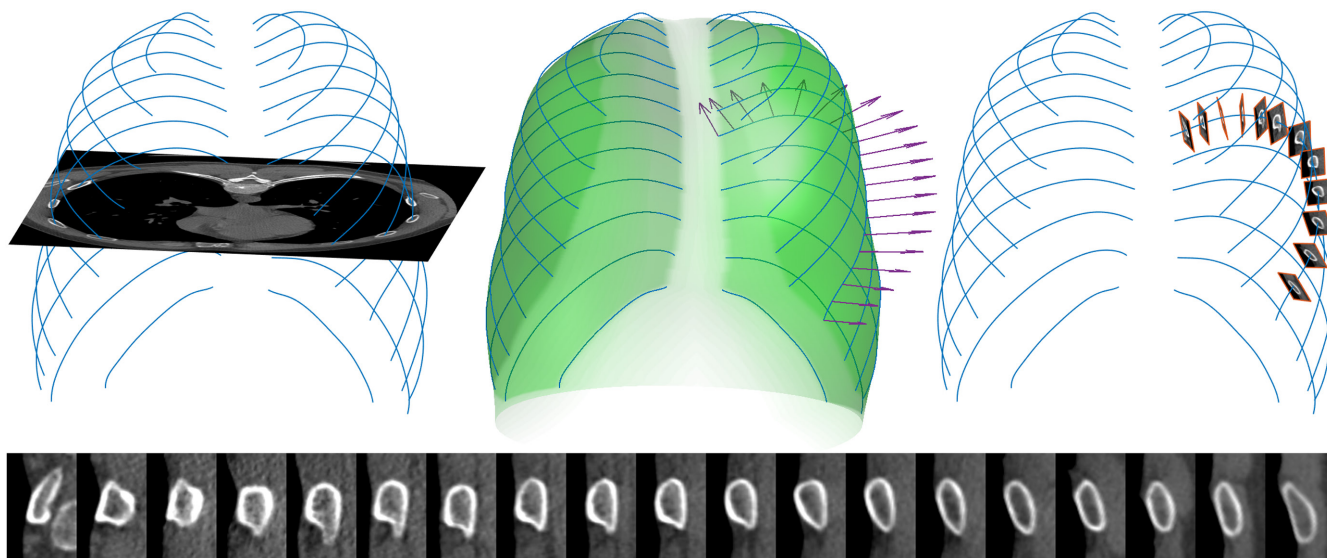


FIGURE 2 3D rib curves (top left) with fitted chest wall surface normals used to align local patch X-axes (top middle), and resulting sampled rib patches (top right and bottom row).

(as defined from within the in-patch view). A superior landmark was then placed at the average between the superior-most border position and the position intersected by a ray extending from the inferior landmark and passing through the periosteal area centroid. Pleural and cutaneous landmarks were placed co-linear with the area centroid and perpendicular to the inferior-superior landmark direction. Along-rib registration between ribs was given directly by the curvilinear percentage length along each rib.

All image processing, data processing, and statistical analyses were performed in MATLAB 2022a (The Mathworks).

2.2 | Zonal analysis

Cortical thickness measurements were collected into per-rib maps (individual grids of $C_{T,TH}$ values registered by along-rib percentage and around-rib location as above). One-dimensional along-rib gaussian smoothing was applied using a symmetric window of 5% of the rib's length. Missing $C_{T,TH}$ values at those regions identified above (4.6% of surface locations) were imputed separately for each rib level using a trimmed scored regression algorithm implemented in the Missing Data Imputation Toolbox (v1.0; Folch-Fortuny et al., 2016).

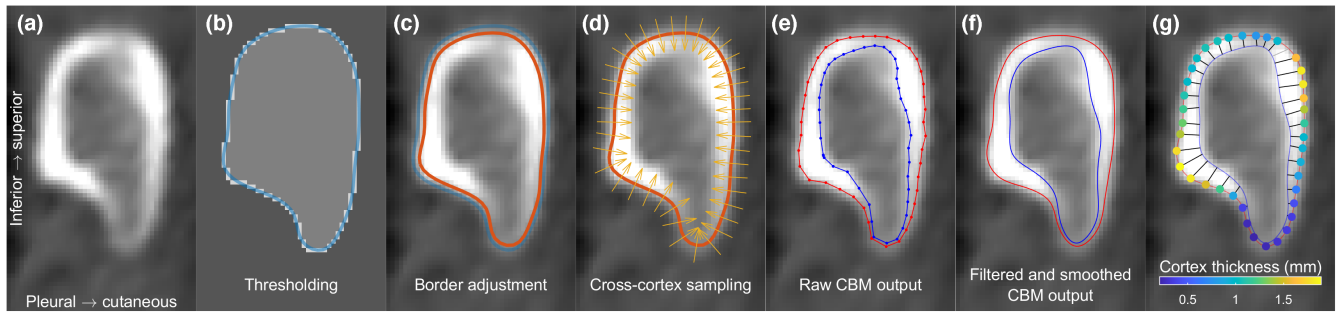


FIGURE 3 Image processing steps from input image patch (a) through to periosteal and endosteal borders (f) and viable cortex thickness measurements (g).

Discrete zones within these maps were identified on each rib corresponding to regional maxima or minima features. These included pleural, cutaneous, inferior, and superior zones all taken from a mid-rib region, as well as a sternal zone covering the full circumference of the distal-most 15% of ribs. Finally, a zone encompassing the rib's full surface was chosen. Average Ct.Th values within each zone were calculated and linear regression was performed to explore the associations between Ct.Th and subject sex and age (along with age \times sex interaction) for each zone and each rib number, with significance assessed at the $p < 0.01$ level to account for repeat analyses.

2.3 | Regional surface analysis

Statistical parametric mapping (SPM) was performed on whole rib Ct.Th surface maps at each rib level using SurfStat (v1.0; Worsley et al., 2009) with linear model terms corresponding to subject age, subject sex, and the age \times sex interaction. Clusters within each map of significant main effects of each term were assessed at the adjusted significance level of $p < 0.05$.

2.4 | Sixth rib validation

To assess the compatibility of results here with past work, the current results for sixth rib Ct.Th values were compared to those previously reported in Holcombe, Kang, Derstine, et al. (2019). Both studies share a similar CBM methodology, but the past results from Holcombe, Kang, Derstine, et al. (2019) were obtained from higher resolution CT scans of 33 excised cadaveric sixth ribs compared to the live subject CT scans that were used here. The previous results were validated against ground truth histological measurements which are unavailable for the live subjects as used in the current study. Therefore, the presence or absence of systematic measurement error in current results was explored by comparing them to results from this validated past work via histogram distributions of whole rib Ct.Th measurements and average Ct.Th values within each discrete rib zone. Subjects from Holcombe, Kang, Derstine, et al. (2019) were on average 10 years older (65 ± 21 years) than the current study cohort so comparisons of average Ct.Th within each

zone were adjusted for the expected difference due to age as predicted by regression analyses from within that same zone.

3 | RESULTS

All pre-processing and CBM were successfully run on 160K image patches from 4014 ribs. Figure 4 shows exemplar results for image patches from the youngest and oldest female subjects.

Average Ct.Th maps from all subjects grouped by rib level are presented in Figure 5 with maps of Ct.Th standard deviation across the population given in Figure A.1. Figure 6 shows those same average Ct.Th maps projected onto exemplar 3D rib geometry. Figure 5 and Figure A.1 also show the superimposed positions of each discrete zone used in subsequent zonal analyses. Each of these Ct.Th maps (and also those separated by sex) including polygon coordinates designating each discrete zone are provided as Supplementary Data S1. Ribs 4 through 8 showed largely equivalent patterns in bone thickness maps across each rib, but with variations in the magnitudes of that thickness. Rib 6 had the thickest cortices of up to 1.6 mm along the pleural aspect. The thinnest cortices were consistently found at the sternal end in all ribs, reaching minimum average values of 0.35 mm in all ribs and as low as 0.30 mm in ribs 2 through 5. Ribs 2 and 3 saw regional Ct.Th maxima that were closer to the vertebral rib ends than for other ribs, and these regional maxima shifted position from a superior rib aspect (nearer to the mid-rib) toward a more pleural rib aspect (nearer to the vertebral end). Figure 6 shows each average Ct.Th map projected onto exemplar 3D rib cage geometry using bi-linear interpolation.

Average Ct.Th values per rib and subject from within each analysis zone are plotted against subject age in Figure 7. Male and female regression lines are included along with each line's slope indicating the mm change in Ct.Th per decade. Predicted Ct.Th values by each regression model at the ages of 20 and 90 years are provided for all ribs and zones in Table 1. Surface maps of the main effects identified from statistical parametric mapping are given in Figure 8. These show the regional variation in the influences of age, sex, and age \times sex interaction model terms on rib surface Ct.Th.

Both zonal (summarized in Figure 7) and regional (summarized in Figure 8) analyses show clear reductions in rib bone thickness with age. In zonal regression models the independent effect of age on

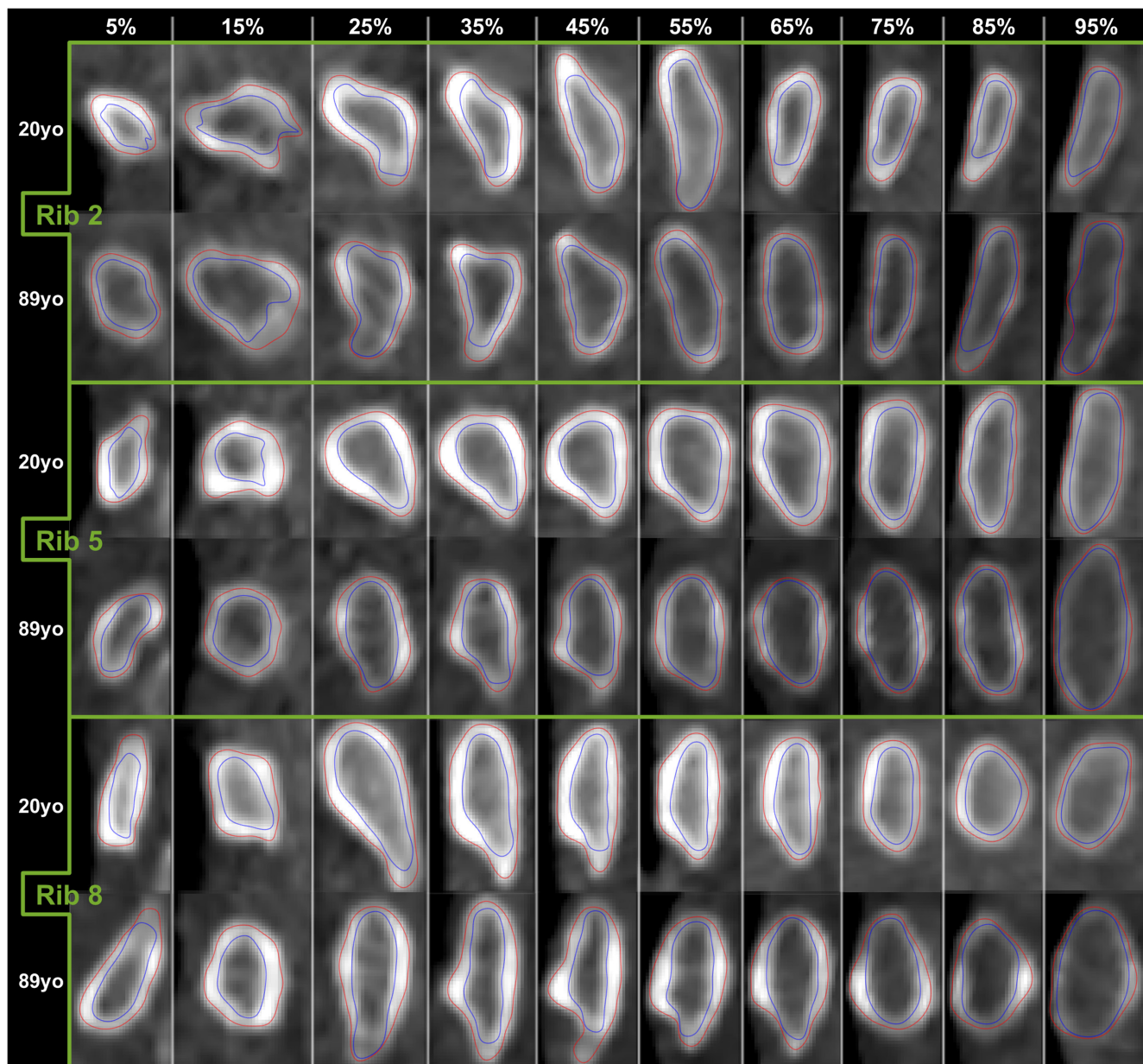


FIGURE 4 Smoothed periosteal and endosteal borders from the youngest and oldest female subjects.

Ct.Th is negative and significant ($p < 0.01$) in all discrete zones of all ribs. This is reflected by large and contiguous clusters of significantly negative regions across rib surfaces in age effect results derived from SPM regional analysis. Typical reduction rates were highest (up to approximately 0.07 mm/decade) in cutaneous and superior rib zones. Reduction rates were lowest in sternal zones, which corresponded with regional analyses showing change with age falling into insignificance toward the sternal extremities of most ribs.

Zonal analysis showed Ct.Th loss with age was higher for females than males in all ribs and all zones, but this difference only reached statistical significance when assessing whole rib zones (all ribs), and cutaneous zones (ribs 2 and 6–11) along with scattered rib levels for other zones (see markers on Figure 7). Regional results were similarly mixed with only scattered clusters for sex-based differences in

the rates of Ct.Th loss reaching significance. Across whole rib zones, female Ct.Th loss occurred at rates approximately 0.015 mm/decade higher than for males ($p < 0.01$ for each rib). This sex-based rate difference was not uniform across all regions, however, with differential Ct.Th loss small (and not significant) along pleural rib aspects and higher (over 0.03 mm/decade, $p < 0.01$) along cutaneous aspects in ribs 6–11.

Generally speaking, zonal regression trend lines (Figure 7) showed that women tended to have thicker cortices than men in the superior and inferior aspects at younger adult ages, and the increased rate of cortical thinning produced a convergence in Ct.Th values at older ages with those of men. Conversely, Ct.Th along the cutaneous aspect was similar in younger men and women, but the higher rate of thinning in women produced a divergence with age which resulted in thinner cortices in older women than in older men.

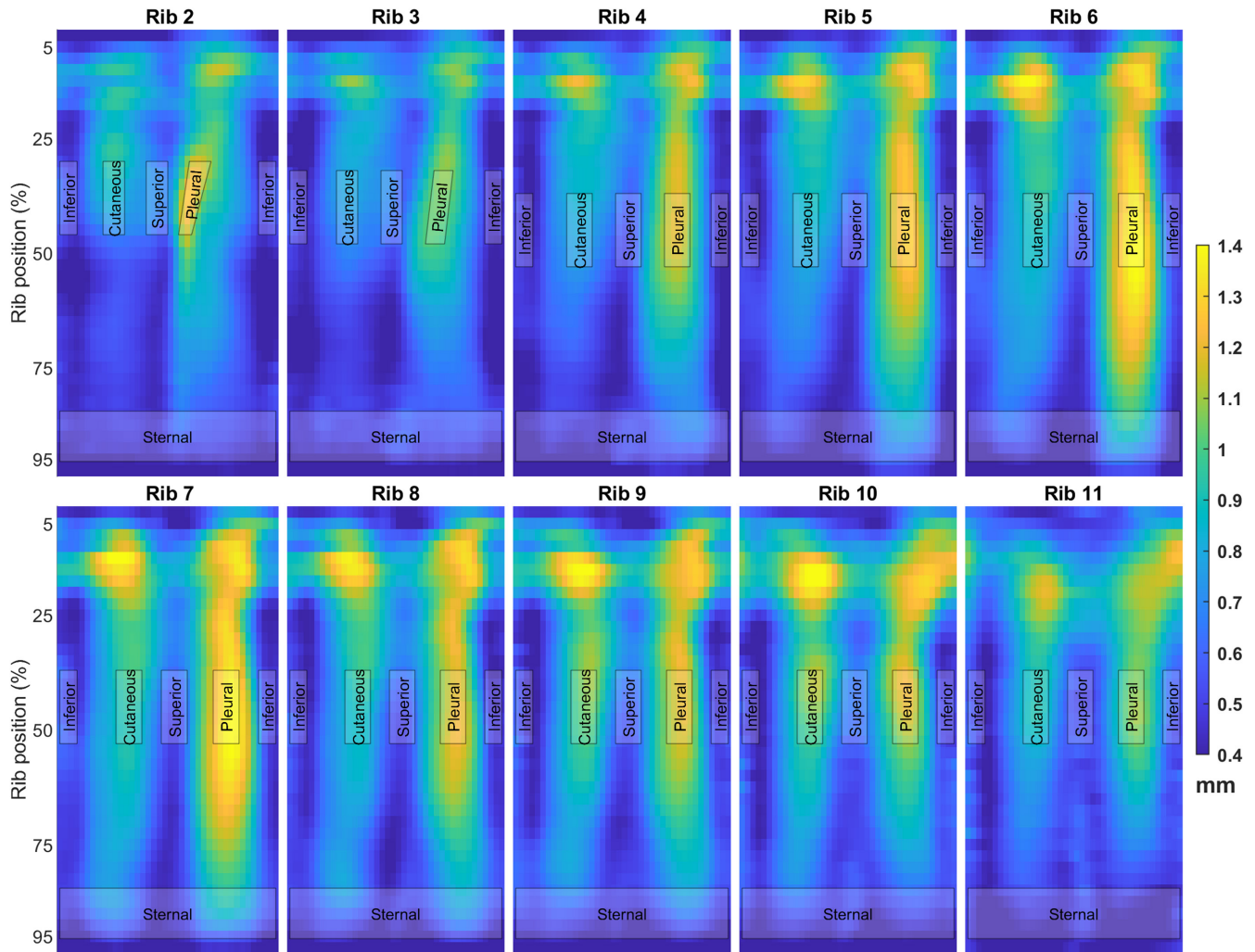


FIGURE 5 Average cortical thickness maps for ribs 2–11 showing the discrete zones chosen for regression analysis.

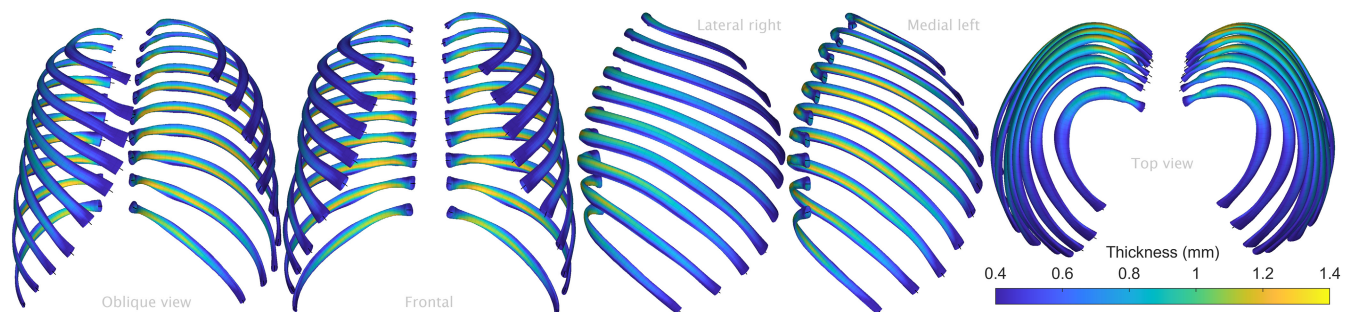


FIGURE 6 Ct.Th maps projected onto exemplar 3D rib cage anatomy.

This phenomenon is further illustrated in Figure 9 showing the main sex effect (after accounting for age \times sex interactions) at 20, 55, and 90 years of age. Sex-based differences in Ct.Th at 20 years of age generally trend toward thicker superior/inferior regions in females and thicker cutaneous/pleural regions in males, but none of these differences are statistically significant at this age apart from small and isolated regions of rib 6. At 55 years, Ct.Th reductions result in cutaneous and pleural regional differences (thinner in females than males) reaching statistical significance across large and connected

portions of most ribs. At this age female ribs still maintain some inferior and superior rib regions that are thicker than males but this difference remains statistically insignificant. By 90 years of age, females tend to have either thinner or near to equal cortices to males across most of each rib's surface, with this difference still only significant in some pleural and cutaneous regions.

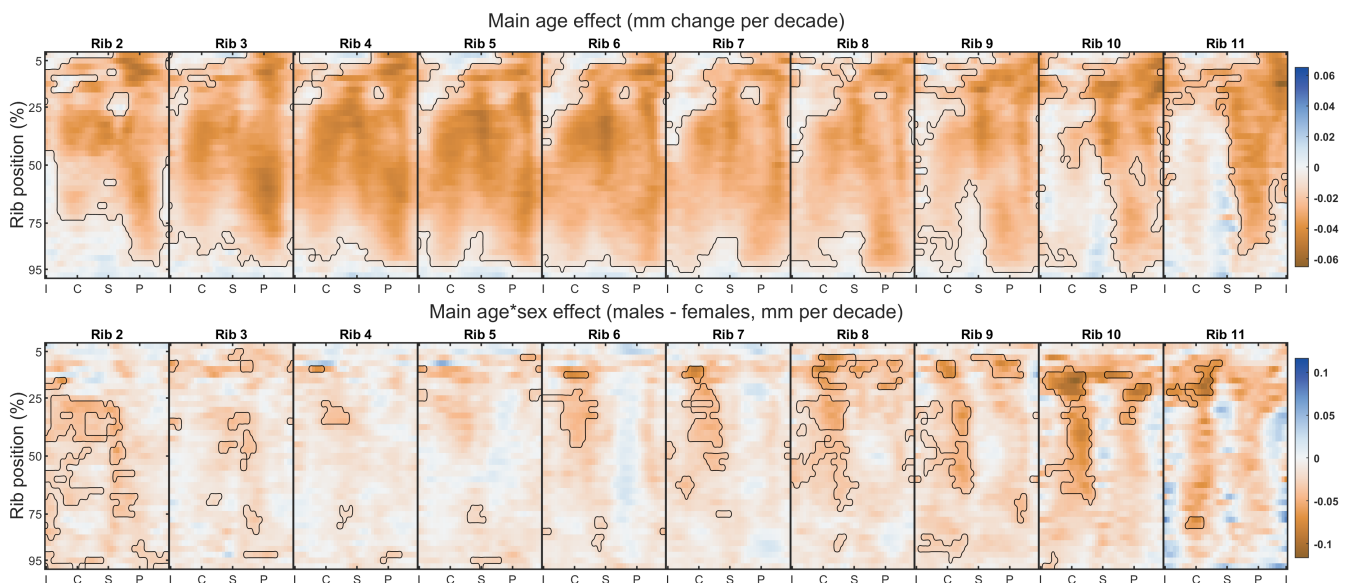
Taken across whole ribs, age, and sex explained between 22% (rib 10) and 37% (rib 2) of the population variability in Ct.Th (Figure 7). Age and sex held most explanatory power in superior (average R^2 across



FIGURE 7 Ct.Th regression models by age for each rib and zone highlighting cortex thinning with senescence. Predicted Ct.Th change per decade is shown for males (blue) and females (red) alongside overall model explanatory power (adjusted R^2 , %). Age was a significant independent predictor of Ct.Th in all models ($p < 0.01$). Rates of cortex thinning were significantly higher in females than males in models marked with (*).

TABLE 1 Predicted cortical thickness values (mm) for males and females at 20 and 90 years of age by rib number and zone.

| Rib | Sex | Pleural | | Cutaneous | | Superior | | Inferior | | Sternal | | Whole rib | |
|-----|-----|---------|------|-----------|------|----------|------|----------|------|---------|------|-----------|------|
| | | 20 | 90 | 20 | 90 | 20 | 90 | 20 | 90 | 20 | 90 | 20 | 90 |
| 2 | F | 1.40 | 0.94 | 1.08 | 0.60 | 0.95 | 0.45 | 0.67 | 0.39 | 0.54 | 0.44 | 0.76 | 0.51 |
| | M | 1.27 | 1.01 | 0.93 | 0.71 | 0.81 | 0.54 | 0.59 | 0.45 | 0.45 | 0.48 | 0.68 | 0.56 |
| 3 | F | 1.25 | 0.79 | 0.95 | 0.48 | 0.88 | 0.40 | 0.60 | 0.34 | 0.57 | 0.45 | 0.75 | 0.46 |
| | M | 1.19 | 0.89 | 0.98 | 0.61 | 0.76 | 0.52 | 0.52 | 0.37 | 0.49 | 0.46 | 0.71 | 0.53 |
| 4 | F | 1.33 | 0.94 | 1.00 | 0.52 | 0.84 | 0.35 | 0.60 | 0.30 | 0.55 | 0.43 | 0.81 | 0.51 |
| | M | 1.31 | 0.97 | 1.00 | 0.64 | 0.77 | 0.41 | 0.53 | 0.32 | 0.53 | 0.47 | 0.79 | 0.56 |
| 5 | F | 1.36 | 1.03 | 1.04 | 0.54 | 0.84 | 0.35 | 0.60 | 0.34 | 0.55 | 0.39 | 0.85 | 0.54 |
| | M | 1.43 | 1.10 | 1.04 | 0.69 | 0.77 | 0.36 | 0.55 | 0.34 | 0.57 | 0.51 | 0.83 | 0.62 |
| 6 | F | 1.48 | 1.13 | 1.10 | 0.58 | 0.86 | 0.37 | 0.68 | 0.39 | 0.59 | 0.44 | 0.90 | 0.59 |
| | M | 1.53 | 1.25 | 1.06 | 0.79 | 0.78 | 0.39 | 0.61 | 0.43 | 0.62 | 0.53 | 0.88 | 0.68 |
| 7 | F | 1.46 | 1.13 | 1.12 | 0.65 | 0.81 | 0.40 | 0.66 | 0.40 | 0.63 | 0.50 | 0.89 | 0.63 |
| | M | 1.51 | 1.29 | 1.07 | 0.87 | 0.71 | 0.42 | 0.57 | 0.45 | 0.66 | 0.57 | 0.87 | 0.71 |
| 8 | F | 1.26 | 0.96 | 1.07 | 0.61 | 0.78 | 0.41 | 0.57 | 0.37 | 0.60 | 0.42 | 0.85 | 0.57 |
| | M | 1.33 | 1.12 | 1.05 | 0.87 | 0.71 | 0.43 | 0.52 | 0.46 | 0.63 | 0.54 | 0.82 | 0.69 |
| 9 | F | 1.22 | 0.90 | 1.13 | 0.71 | 0.82 | 0.45 | 0.58 | 0.39 | 0.57 | 0.39 | 0.84 | 0.57 |
| | M | 1.31 | 1.12 | 1.18 | 1.07 | 0.77 | 0.46 | 0.55 | 0.46 | 0.58 | 0.55 | 0.83 | 0.71 |
| 10 | F | 1.22 | 0.88 | 1.12 | 0.70 | 0.83 | 0.52 | 0.56 | 0.42 | 0.52 | 0.37 | 0.85 | 0.58 |
| | M | 1.24 | 1.11 | 1.11 | 1.17 | 0.79 | 0.48 | 0.51 | 0.44 | 0.54 | 0.51 | 0.78 | 0.71 |
| 11 | F | 1.17 | 0.74 | 0.83 | 0.60 | 0.66 | 0.43 | 0.63 | 0.43 | 0.44 | 0.38 | 0.75 | 0.51 |
| | M | 1.25 | 0.93 | 0.94 | 1.02 | 0.61 | 0.45 | 0.62 | 0.44 | 0.46 | 0.44 | 0.75 | 0.64 |

FIGURE 8 Main age and age×sex effects on regional Ct.Th. Rib surface clusters exhibiting effects significantly different to zero ($p < 0.05$) are delineated by black contours.

all ribs of 29%) and cutaneous (avg. $R^2 = 25\%$) rib regions, whereas associations in pleural, inferior, and sternal regions were less strong (avg. R^2 around 12%).

The zonal regression models presented above each included a linear age term and an interaction term between age and sex.

Inspection of residuals from these fitted models did not show trends with subject age, and the addition of quadratic regression terms (i.e., squared-age) offered little to no improvement in adjusted R^2 model explanatory power. This indicates that the rate of cortical thinning per decade remained constant. In other words, while the bone

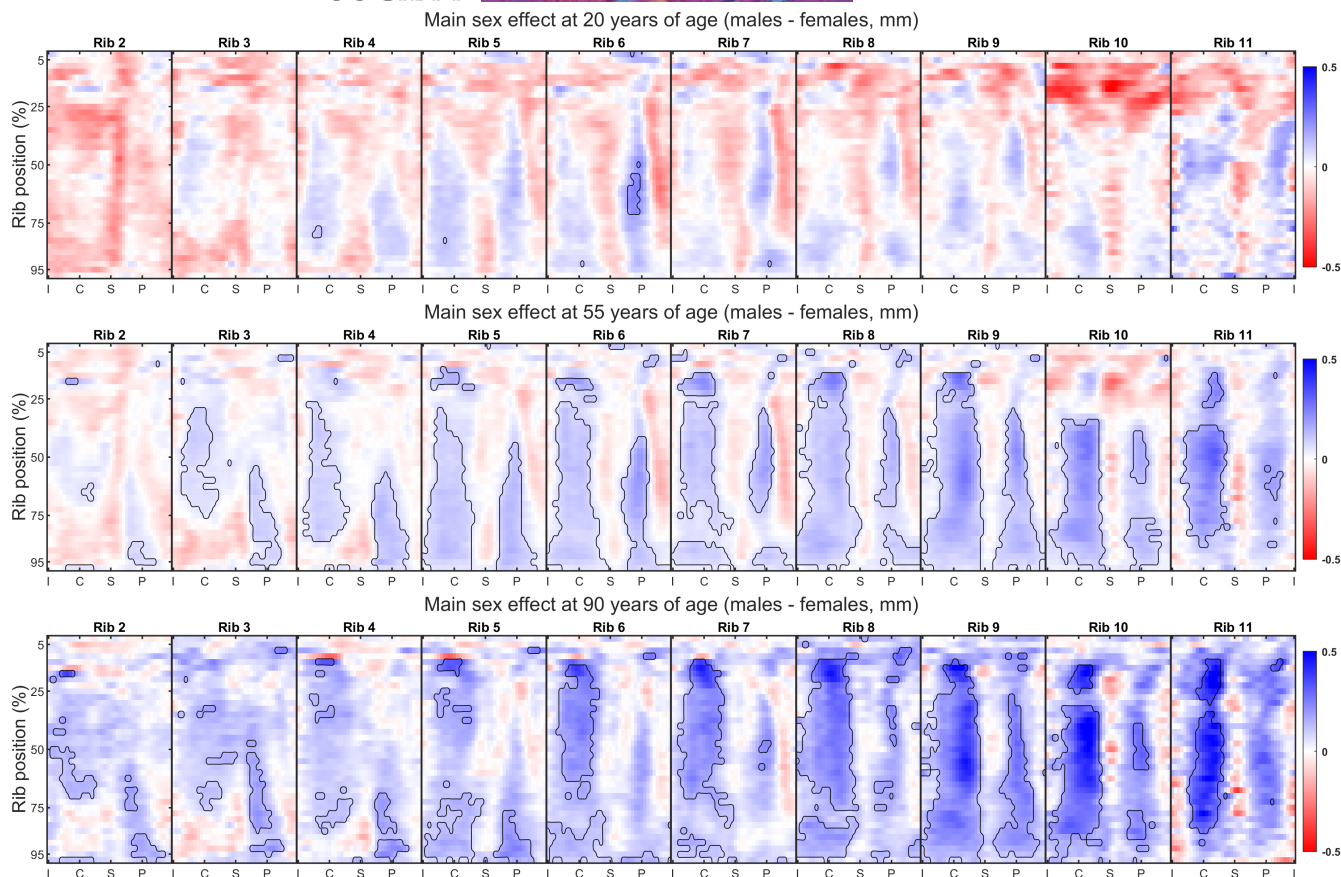


FIGURE 9 Main sex effects on regional Ct.Th at 20, 55, and 90 years of age. Rib surface clusters exhibiting significant differences ($p < 0.05$) are delineated by black contours.

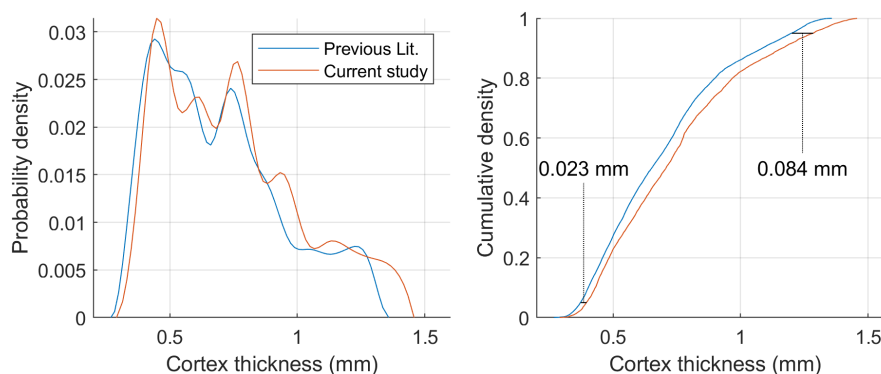


FIGURE 10 Histogram (left) and cumulative density function (right) of average sixth Ct.Th map values compared to past literature (Holcombe, Kang, Derstine, et al., 2019). The current study shows a thickness increase comparable to that expected from subjects who are on average 10 years younger than the reference cohort.

content loss was higher for females than for males, the data did not suggest an acceleration in this loss with advancing age for either sex.

The average sixth rib Ct.Th map from this study (Figure 5) shared overall patterns with a previously published rib 6 thickness map from Holcombe, Kang, Derstine, et al. (2019). Figure 10 presents a comparison of histograms and cumulative density function plots of all Ct.Th values from these two maps. These show current Ct.Th results being between 0.02 mm higher (in thinner regions) and 0.08 mm

higher (in thicker regions) than the established reference. Given the 10-year difference in cohort ages between the two studies (which from Figure 7 corresponds to between 0.01 mm and 0.06 mm difference in Ct.Th), current results are seen to match well with this previously validated study. Further zonal-based comparison is provided in Figure 11 which shows that average Ct.Th values found within every zone match—particularly after adjustment for cohort age—to within 1 standard deviation as determined by the current study.

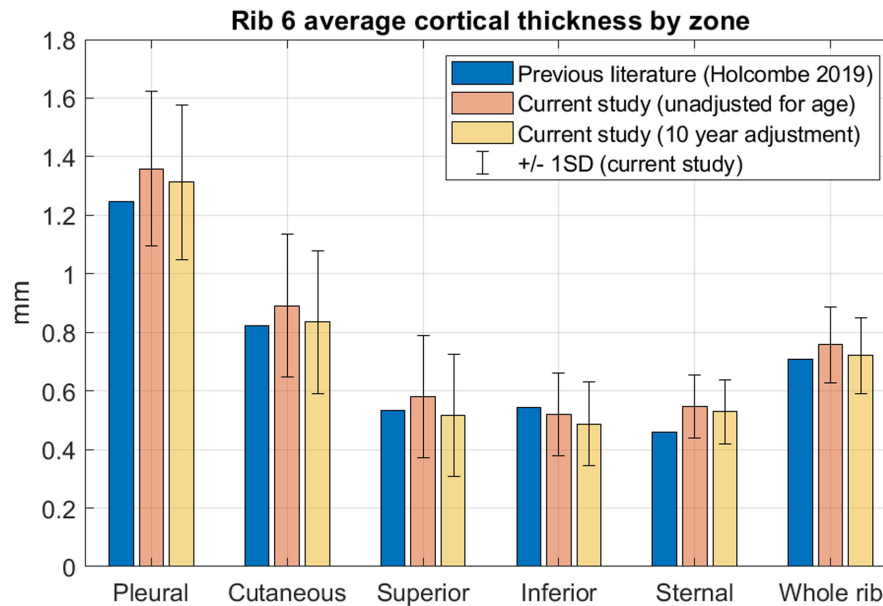


FIGURE 11 Comparison by zone of average rib 6 Ct.Th in previously validated literature (Holcombe, Kang, Derstine, et al., 2019) to current results.

4 | DISCUSSION

Here, we have assessed cortical bone thickness from over 4000 ribs of 240 adult subjects and analyzed thickness associations with sex, age, and anatomic location. To the authors' knowledge, this is the largest subject pool from which detailed average thickness values have been drawn, and the first to quantify regional rates of bone loss in the ribs with advancing age.

The measurement techniques used in this study are adapted from Holcombe, Kang, Derstine, et al. (2019) with additional pre-processing steps to obtain consistent and registered patch images from live-subject clinical scans, and additional post-processing steps to output smoothed periosteal and endosteal borders. That previous study used excised sixth ribs scanned at a high resolution ($0.15 \times 0.15 \times 0.67$ mm), and showed mean/sd error of the CBM technique compared to histological measurements of -0.013 ± 0.167 mm. Results in Figures 10 and 11 show regional trends and overall Ct.Th magnitudes that are compatible with this previously validated use of CBM methodology, particularly after accounting for population age differences between the two studies. When contrasting these result differences (usually between 0.01 and 0.05 mm) to our overall population standard deviation (0.11–0.26 mm, Figure 11), we can be reassured that systematic biases due to methodological factors like changing CT resolutions, smoothing techniques, and scanning of live subjects are likely small when compared to overall population variance due to individuality. Similarly, previous experimental studies (Agnew et al., 2015, 2018; Kemper et al., 2009) are seen to be compatible with current results having measured average rib thicknesses (albeit aggregated across multiple ribs and from varying positions along and around those ribs) at pleural, cutaneous, inferior, and superior areas to be approximately 1.15, 0.75, 0.43, and 0.46 mm, respectively.

Results from Figure 5 show distinct patterns in cortical bone thickness that differ even between adjacent ribs, particularly for higher ribs 2 and 3. A unique aspect of the second rib is a tuberosity on its superior surface which forms part of the origin for the serratus anterior muscle which inserts onto the upper part of the scapula as well as the posterior scalene muscle which connects to cervical vertebrae (Safarini & Bordoni, 2022). A well-established mechanism for bone adaptation is the cyclic forces exerted on muscle origin and insertion sites from muscle activation, and the regional maxima in rib 2 Ct.Th values correspond well with this attachment site. For consistency, the second rib regional Ct.Th maxima (demarcated as pleural zone) was shifted superiorly to match this local rib 2 feature. Overall, all results from the current study should be taken in context with each rib's muscle attachment sites and their potential effect on local bone thickness in mind. In ribs 4–9, the overall patterns in thickness maps were largely consistent albeit with inter-rib variations in Ct.Th magnitude. These ribs saw mid-rib maxima at both pleural and cutaneous aspects and minima along superior and inferior aspects. These ribs also follow largely similar patterns in muscle attachments via the intercostal muscle layers and two or more of the pectoralis minor muscles, external abdominal oblique muscles, and serratus anterior muscles (De Troyer et al., 2005; Safarini & Bordoni, 2022). It should also be noted that Ct.Th measurements along the inferior aspect of a rib can be complicated by the presence of an elongated costal groove. This inferior elongation was observed between approximately 20%–60% along the lengths of ribs 3–10 with the greatest prominence at the 30% location but showed wide variation both regionally and between subjects. It is commonly thought to protect the neurovascular bundle running along its deep surface. In the current study, the full periosteal border was used, but in rib patches where this groove is particularly pronounced the underlying assumption that the cortex is comprised two approximately concentric

borders break down. Steps were taken to discard Ct.Th observations crossing the full groove cortex in such cases, but this variation led to greater Ct.Th variability along the mid-rib inferior aspect (Figure 7). Care should be taken when applying rib Ct.Th results in these regions to generalized rib geometry as measurements are likely biased toward those found in subjects with less prominent costal grooves.

A notable result from the current study is that while rates of bone thinning varied regionally, they did not do so simply as a percentage of local thickness. For example, at up to 1.6 mm the average cortices along pleural rib aspects were over twice as thick as those along superior rib aspects, yet their rates of thinning were lower than those seen along superior and cutaneous aspects in both men and women. Furthermore, males (who were both heavier and taller) did not generally possess thicker rib cortices than females except in older cohorts. In fact, in younger cohorts and at some locations (primarily superior and inferior aspects), female rib cortices tended to be thicker on average than male cortices. This goes some way to explain the high inter-subject variability and lack of clear trends with age (Agnew et al., 2018) and sex (Holcombe, Kang, Derstine, et al., 2019) that were found in previous studies.

The along-rib registration used in this study is a simple and repeatable normalization of ribs along their curvilinear length. It should be noted though the potential for systematic misregistration (Gee & Treece, 2014) if ribs of certain population subgroups have topology discordance with this linear scheme in a systematic way. For example, males or females may systematically differ in the relative along-rib positions of their costal grooves such that misalignment of this anatomical feature occurs after normalizing by rib length. Similarly, rotational alignment is based partly on the cross-sectional shape of ribs which may also have systematic differences across the population. While attempts have been made in the current study to produce repeatable registration procedures to normalize inter-subject anatomy, such systematic misregistration has not been fully investigated and should be considered when applying the current results.

The sex-based, region-based, and age-based differences in Ct.Th found here have implications for future modeling of rib fractures and subsequent thoracic injuries. For example, Palanca et al. (2022) found that ribs with thicker cortices were more likely to exhibit a brittle break (which can further damage surrounding tissues) rather than buckle during compressive loading. Iraeus et al. (2019) also found that better cortex definitions offered improvements in predicting the force required and resulting locations of rib fractures. Results here can inform representative sex- or age-specific models and do so with greater detail than has previously been available in full-body HBMs.

It is important to also consider the limitations of the present work. Firstly, the study is designed to infer longitudinal changes with age but does so via cross-sectional observations of different individuals at various single points during their lifetime. This is a necessary compromise to make given the absence of appropriate and repeated CT scans available from healthy subjects across spans of many decades. Secondly, the adult cohort was drawn from a Midwestern US

population, so there was limited ability to explore potential variation associated with subject ancestry. We also chose to exclude the first and twelfth ribs from the current analysis. While the first rib is important and plays a key role in interaction with safety systems, its morphology is entirely distinct from other ribs and does not directly lend itself to the same registration techniques used here so should be addressed separately. Twelfth ribs were excluded due to their small but varied size, and they are also not thought to play a substantial structural role during loading from blunt trauma events.

5 | CONCLUSION

Here, we have applied a cortical bone mapping methodology to ribs in clinical CT scans taken from a US adult population of broadly sampled ages. The resulting maps of cortical thickness across the surfaces of ribs 2–11 can be directly applied to improve the biofidelity of current finite element HBMs. Results also highlight the regional variation in cortical bone thinning that occurs with advancing age, allowing for further specification of such models to represent males or females across full adult lifespans. Given appropriate CT availability, the techniques used in this study can further be applied clinically to assess-specific rib bone characteristics and their relationships with injury risk, disease progression, or therapy response.

CONFLICT OF INTEREST

The authors report that there are no conflicts of interest that might affect this work. The anonymized and retrospective scan data used in this study were obtained under IRB HUM00041441.

DATA AVAILABILITY STATEMENT

The data that supports the findings of this study are available in the Supplementary Material of this article.

ORCID

Sven A. Holcombe  <https://orcid.org/0000-0003-0795-7019>

Brian A. Derstine  <https://orcid.org/0000-0002-2869-9584>

REFERENCES

- Agnew, A.M., Schafman, M., Moorhouse, K., White, S.E. & Kang, Y.-S. (2015) The effect of age on the structural properties of human ribs. *Journal of the Mechanical Behavior of Biomedical Materials*, 41, 302–314. Available from: <https://doi.org/10.1016/j.jmbbm.2014.09.002>
- Agnew, A.M., Murach, M.M., Dominguez, V.M., Sreedhar, A., Misicka, E., Harden, A. et al. (2018) Sources of variability in structural bending response of pediatric and adult human ribs in dynamic frontal impacts. *Stapp Car Crash Journal*, 62, 119–192.
- Alswat, K.A. (2017) Gender disparities in osteoporosis. *Journal of Clinical Medicine Research*, 9, 382–387. Available from: <https://doi.org/10.14740/jocmr2970w>
- Chen, H. (2014) Bone three-dimensional microstructural features of the common osteoporotic fracture sites. *World Journal of Orthopedics*, 5, 486–495. Available from: <https://doi.org/10.5312/wjo.v5.i4.486>
- Chen, H., Poulard, D., Forman, J., Crandall, J. & Panzer, M.B. (2018) Evaluation of geometrically personalized THUMS pedestrian model response against sedan–pedestrian PMHS impact test data.

- Traffic Injury Prevention*, 19, 542–548. Available from: <https://doi.org/10.1080/15389588.2018.1450979>
- Choi, H.-Y. & Kwak, D.-S. (2011) Morphologic characteristics of Korean elderly rib. *Journal of Automotive Safety and Energy*, 2, 112–127.
- De Troyer, A., Kirkwood, P.A. & Wilson, T.A. (2005) Respiratory action of the intercostal muscles. *Physiological Reviews*, 85, 717–756. Available from: <https://doi.org/10.1152/physrev.00007.2004>
- Dogrul, B.N., Kiliccalan, I., Asci, E.S. & Peker, S.C. (2020) Blunt trauma related chest wall and pulmonary injuries: an overview. *Chinese Journal of Traumatology*, 23, 125–138. Available from: <https://doi.org/10.1016/j.cjtee.2020.04.003>
- Eftekhar-Sadat, B., Ghavami, M., Toopchizadeh, V. & Ghahvechi Akbari, M. (2016) Wrist bone mineral density utility in diagnosing hip osteoporosis in postmenopausal women. *Therapeutic Advances in Endocrinology and Metabolism*, 7, 207–211. Available from: <https://doi.org/10.1177/2042018816658164>
- Folch-Fortuny, A., Arteaga, F. & Ferrer, A. (2016) Missing data imputation toolbox for MATLAB. *Chemometrics and Intelligent Laboratory Systems*, 154, 93–100. Available from: <https://doi.org/10.1016/j.chemolab.2016.03.019>
- Forman, J., Poplin, G.S., Shaw, C.G., McMurry, T.L., Schmidt, K., Ash, J. et al. (2019) Automobile injury trends in the contemporary fleet: belted occupants in frontal collisions. *Traffic Injury Prevention*, 20, 607–612. Available from: <https://doi.org/10.1080/15389588.2019.1630825>
- Gee, A.H. & Treece, G.M. (2014) Systematic misregistration and the statistical analysis of surface data. *Medical Image Analysis*, 18, 385–393. Available from: <https://doi.org/10.1016/j.media.2013.12.007>
- Holcombe, S.A., Wang, S.C. & Grotberg, J.B. (2017) The effect of age and demographics on rib shape. *Journal of Anatomy*, 231, 229–247. Available from: <https://doi.org/10.1111/joa.12632>
- Holcombe, S.A., Hwang, E., Derstine, B.A. & Wang, S.C. (2018) Measuring rib cortical bone thickness and cross section from CT. *Medical Image Analysis*, 49, 27–34. Available from: <https://doi.org/10.1016/j.media.2018.07.003>
- Holcombe, S.A., Kang, Y., Derstine, B.A., Wang, S.C. & Agnew, A.M. (2019) Regional maps of rib cortical bone thickness and cross-sectional geometry. *Journal of Anatomy*, 235, 883–891. Available from: <https://doi.org/10.1111/joa.13045>
- Holcombe, S.A., Kang, Y.-S.S., Wang, S.C. & Agnew, A.M. (2019) The accuracy of local rib bone geometry measurement using full body CT images. *International Research Council on the Biomechanics of Injury*, 19, 64.
- Holcombe, S.A., Agnew, A.M., Derstine, B. & Wang, S.C. (2020) Comparing FE human body model rib geometry to population data. *Biomechanics and Modeling in Mechanobiology*, 19, 2227–2239. Available from: <https://doi.org/10.1007/s10237-020-01335-2>
- Hwang, E., Hu, J. & Reed, M.P. (2020) Validating diverse human body models against side impact tests with post-mortem human subjects. *Journal of Biomechanics*, 98, 109444. Available from: <https://doi.org/10.1016/j.jbiomech.2019.109444>
- Iraeus, J., Lundin, L., Storm, S., Agnew, A., Kang, Y.-S., Kemper, A. et al. (2019) Detailed subject-specific FE rib modeling for fracture prediction. *Traffic Injury Prevention*, 20, S88–S95. Available from: <https://doi.org/10.1080/15389588.2019.1665649>
- Kemper, A.R., McNally, C., Kennedy, E.A., Manoogian, S.J., Rath, A.L., Ng, T.P. et al. (2005) Material properties of human rib cortical bone from dynamic tension coupon testing. *Stapp Car Crash Journal*, 49, 199–230.
- Kemper, A.R., McNally, C., Pullins, C.A., Freeman, L.J., Duma, S.M. & Rouhana, S.M. (2007) The biomechanics of human ribs: material and structural properties from dynamic tension and bending tests. *Stapp Car Crash Journal*, 51, 235–273.
- Kemper, A.R., Stitzel, J.D., McNally, C., Gabler, H.C. & Duma, S.M. (2009) Biomechanical response of the human clavicle: the effects of loading direction on bending properties. *Journal of Applied Biomechanics*, 25, 165–174. Available from: <https://doi.org/10.1123/jab.25.2.165>
- Li, Z., Kindig, M., Subit, D. & Kent, R. (2010) Development of finite element model of 50th percentile male using multiblock hex meshing approach. In: *38th Proceedings of the 6th annual world congress on biomechanics*. Washington, DC: National Highway Traffic Safety Administration (NHTSA). <https://www-nrd.nhtsa.dot.gov/database/bio/proceedings/search.asp>
- Mohr, M., Abrams, E., Engel, C., Long, W.B. & Bottlang, M. (2007) Geometry of human ribs pertinent to orthopedic chest-wall reconstruction. *Journal of Biomechanics*, 40, 1310–1317. Available from: <https://doi.org/10.1016/j.jbiomech.2006.05.017>
- Murach, M.M., Kang, Y.-S., Goldman, S.D., Schafman, M.A., Schlecht, S.H., Moorhouse, K. et al. (2017) Rib geometry explains variation in dynamic structural response: potential implications for frontal impact fracture risk. *Annals of Biomedical Engineering*, 45, 2159–2173. Available from: <https://doi.org/10.1007/s10439-017-1850-4>
- Palanca, M., Liebsch, C., Hübner, S., Marras, D., Ruspi, M.L., Marconi, F. et al. (2022) Global and local characterization explains the different mechanisms of failure of the human ribs. *Journal of the Mechanical Behavior of Biomedical Materials*, 125, 104931. Available from: <https://doi.org/10.1016/j.jmbbm.2021.104931>
- Pignolo, R.J., Law, S.F. & Chandra, A. (2021) Bone aging, cellular senescence, and osteoporosis. *JBMR Plus*, 5, e10488 Available from: <https://doi.org/10.1002/jbm4.10488>
- Pipkorn, B., Iraeus, J., Lindkvist, M., Puthan, P. & Bunketorp, O. (2020) Occupant injuries in light passenger vehicles—a NASS study to enable priorities for development of injury prediction capabilities of human body models. *Accident Analysis & Prevention*, 138, 105443. Available from: <https://doi.org/10.1016/j.aap.2020.105443>
- Poole, K.E.S., Treece, G.M., Mayhew, P.M., Vaculik, J., Dungal, P., Horák, M. et al. (2012) Cortical thickness mapping to identify focal osteoporosis in patients with hip fracture. *PLoS One*, 7, e38466. Available from: <https://doi.org/10.1371/journal.pone.0038466>
- Safarini, O.A. & Bordoni, B. (2022) *Anatomy, thorax, ribs*. StatPearls [Internet]. Treasure Island, FL: StatPearls Publishing. <http://www.ncbi.nlm.nih.gov/books/NBK538328/>
- Schoell, S.L., Weaver, A.A., Vavalle, N.A. & Stitzel, J.D. (2015) Age- and sex-specific thorax finite element model development and simulation. *Traffic Injury Prevention*, 16, S57–S65. Available from: <https://doi.org/10.1080/15389588.2015.1005208>
- Shi, X., Cao, L., Reed, M.P., Rupp, J.D., Hoff, C.N. & Hu, J. (2014) A statistical human rib cage geometry model accounting for variations by age, sex, stature and body mass index. *Journal of Biomechanics*, 47, 2277–2285. Available from: <https://doi.org/10.1016/j.jbiomech.2014.04.045>
- Sirmali, M., Türüt, H., Topçu, S., Gülhan, E., Yazici, U., Kaya, S. et al. (2003) A comprehensive analysis of traumatic rib fractures: morbidity, mortality and management. *European Journal of Cardio-Thoracic Surgery*, 24, 133–138.
- Sozen, T., Ozisik, L. & Calik Basaran, N. (2017) An overview and management of osteoporosis. *European Journal of Rheumatology*, 4, 46–56. Available from: <https://doi.org/10.5152/eurjrheum.2016.048>
- Stawicki, S.P., Grossman, M.D., Hoey, B.A., Miller, D.L. & Reed, J.F. (2004) Rib fractures in the elderly: a marker of injury severity. *Journal of the American Geriatrics Society*, 52, 805–808. Available from: [10.1111/j.1532-5415.2004.52223.x](https://doi.org/10.1111/j.1532-5415.2004.52223.x)
- Talbot, B.S., Gange, C.P., Chaturvedi, A., Klionsky, N., Hobbs, S.K. & Chaturvedi, A. (2017) Traumatic rib injury: patterns, imaging pitfalls, complications, and treatment. *Radiographics*, 37, 628–651. Available from: <https://doi.org/10.1148/rg.2017160100>
- Telfer, S., Brunnuell, C.L., Allen, J.D., Linnax, K.F., Zamora, D. & Kleweno, C.P. (2021) The effect of age and sex on pelvic bone density measured opportunistically in clinical CT scans. *Journal of Orthopaedic*

Research, 39, 485–492. Available from: <https://doi.org/10.1002/jor.24792>

Treece, G.M. & Gee, A.H. (2015) Independent measurement of femoral cortical thickness and cortical bone density using clinical CT. *Medical Image Analysis*, 20, 249–264. Available from: <https://doi.org/10.1016/j.media.2014.11.012>

Vavalle, N.A., Schoell, S.L., Weaver, A.A., Stitzel, J.D. & Gayzik, F.S. (2014) Application of radial basis function methods in the development of a 95th percentile male seated FEA model. *Stapp Car Crash Journal*, 58, 361–384.

Witt, C.E. & Bulger, E.M. (2017) Comprehensive approach to the management of the patient with multiple rib fractures: a review and introduction of a bundled rib fracture management protocol. *Trauma Surgery & Acute Care Open*, 2, e000064. Available from: <https://doi.org/10.1136/tsaco-2016-000064>

Worsley, K., Taylor, J., Carbonell, F., Chung, M., Duerden, E., Bernhardt, B. et al. (2009) SurfStat: a Matlab toolbox for the statistical analysis of univariate and multivariate surface and volumetric

data using linear mixed effects models and random field theory. *NeuroImage*, 47, S102. Available from: [https://doi.org/10.1016/S1053-8119\(09\)70882-1](https://doi.org/10.1016/S1053-8119(09)70882-1)

SUPPORTING INFORMATION

Additional supporting information can be found online in the Supporting Information section at the end of this article.

How to cite this article: Holcombe, S.A. & Derstine, B.A. (2022) Rib cortical bone thickness variation in adults by age and sex. *Journal of Anatomy*, 241, 1344–1356. Available from: <https://doi.org/10.1111/joa.13751>

APPENDIX A

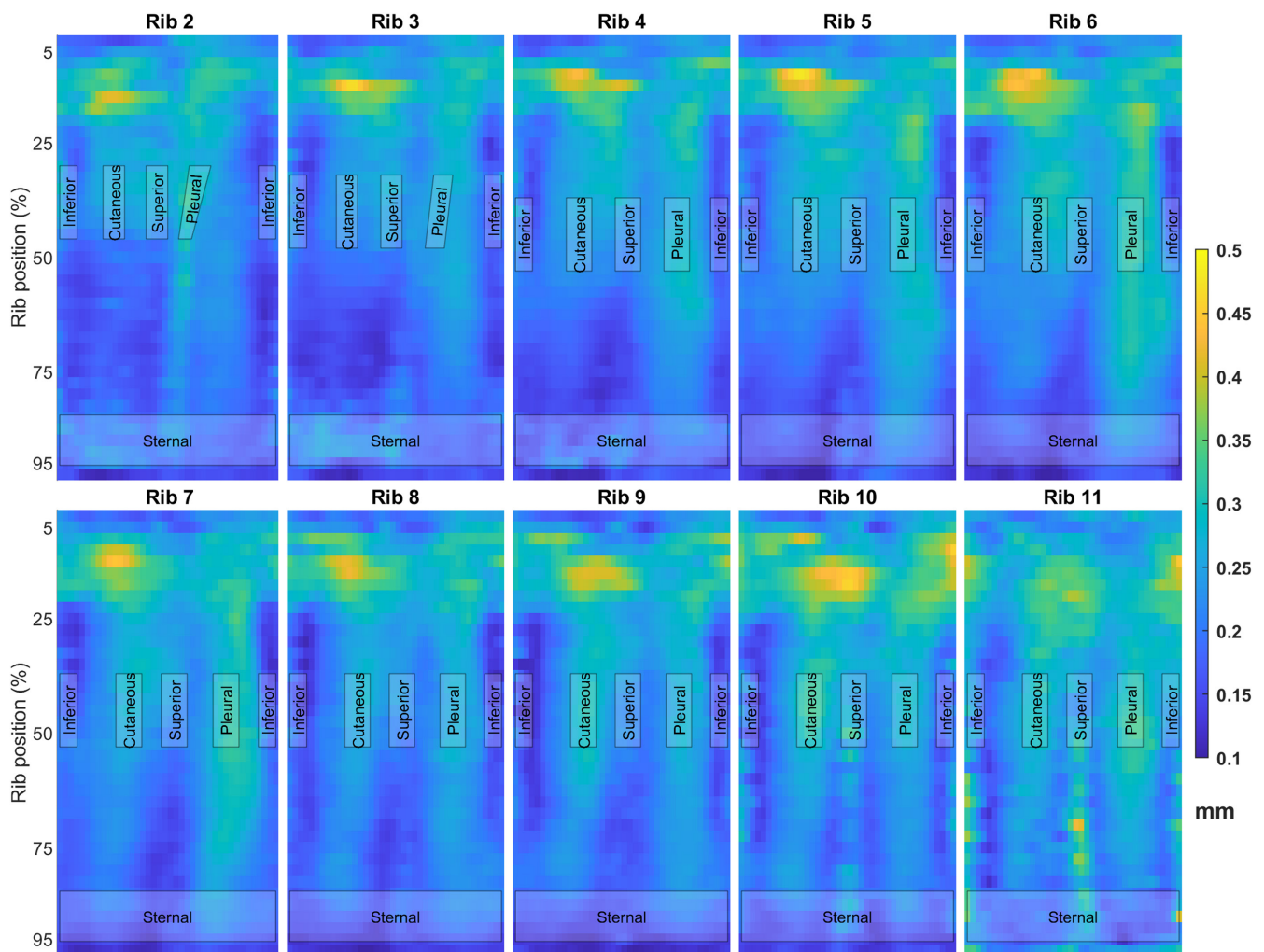


FIGURE A.1 Cortical thickness standard deviation maps for ribs 2–11.